Spectroscopic (IR and Raman) Analysis and Density Functional Theory (DFT) Investigation on Cyclohexanone Oxime

Sagar Sharma[1], Kamal Khanal[2]*
[1,2]Oxford Secondary School, Butwal, Nepal, [2]Butwal Multiple Campus, Butwal, Nepal
Corresponding author: kamal.khanal@bumc.tu.edu.np
Received: Aug 3, Reviewed: Oct 11. Revised: Oct15, Accepted: Dec 16

Abstract

In this research, the molecular, electronic, and spectroscopic properties of cyclohexanone oxime were investigated using density functional theory (DFT) in both the gas phase and solvents (water, DMSO, and ethanol) at the B3LYP/6-311++G (d,p) level of theory. HOMO-LUMO energy calculations showed higher stability of cyclohexanone oxime in solvent phases than in the gas phase due to a larger energy gap in solvents (6.66 eV) compared to the gas phase (6.45 eV). Thermodynamic parameters, molecular electrostatic potential (MEP) maps, density of states (DOS) spectra, and Mulliken atomic charges were investigated to gain a broad understanding of the physicochemical behavior of the cyclohexanone oxime molecule. Further analysis included non-covalent interaction (NCI) and reduced density gradient (RDG) plots to understand weak interactions, and Fukui function calculations to identify different reactive sites in the cyclohexanone oxime molecule. Spectroscopic properties were studied by simulating FT-IR, FT-Raman, and UV-Vis spectra. All these parameters were then compared with all the available experimental results on the cyclohexanone oxime compound. These comprehensive theoretical investigations provided valuable information on the structural, electronic, and spectroscopic features of the cyclohexanone oxime molecule, highlighting the influence of different solvent environments on its behavior.

Keywords: Spectroscopy, HOMO-LUMO, NCI-RDG, Fukui function, DOS spectra

Introduction

N-cyclohexylidenehydroxylamine, commonly called as Cyclohexanone Oxime (CHO), is a white crystalline solid with molecular formula $C_6H_{11}NO$, molecular weight 113.16 a.u., and a melting point of 90^0C. CHO is mainly used as a significant intermediate compound in the production of caprolactam, a key monomer of Nylon-6. CHO is soluble in water and ethanol (Lide, 1992; Sharp et al., 2024). CHO is produced by condensation of cyclohexanone with hydroxylamine sulphate or hydroxylamine phosphate (Fisher and Cresentini, 1985; Sumathi et al., 2025). It has been extensively used for various industrial applications, particularly in the Beckmann rearrangement (Zhang et al., 2014). CHO is also considered to be an intermediate compound in the oxidative metabolism of sodium cyclamate, which is an artificial sweetener (Unger and McMahon, 1981). Because of the presence of the oxime (=NOH) functional group (Sumathi et al., 2024), the cyclohexanone oxime molecule shows interesting structural, electronic, and reactive properties that make it a valuable subject for various computational and spectroscopic investigations. The chemical structure of

cyclohexanone oxime is depicted in Figure 1.

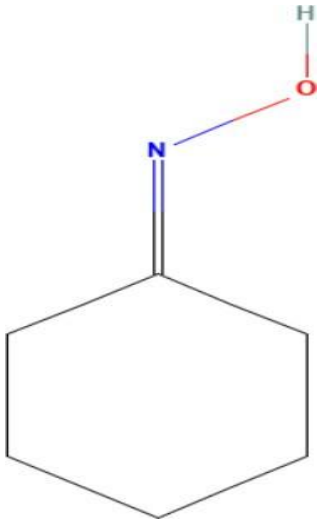

Figure 1: Chemical Structure of Cyclohexanone Oxime (PubChem Compound Database, CID:7517)

Recently, various computational studies on compounds with synthetic, medicinal, life science-based, agro-based, or industrial significance have caught the eye of many researchers in the field of physics and chemistry. Similarly, CHO as well as its polysubstituted compounds have gone through many computational studies, like in the research article on Gaussian hybrid computational analysis of CHO in the gas phase, where the DFT method was used to understand its physicochemical properties (Ramalingam et al., 2012; Murugavel et al., 2023). Thermodynamic properties of CHO in the gas phase via DFT (B3LYP/6-311++G (d,p)) calculations show that the calculated values and the experimental value of entropy agreed with 1% difference (Kozyro et al., 1992). To date, no comprehensive theoretical investigation of cyclohexanone oxime insolvent media such as water, ethanol, and DMSO has been reported. Most existing studies have concentrated on its gas phase characteristics, while solvent effects, non-covalent interactions, and molecular reactivity aspects remain insufficiently explored. To bridge these gaps, the present work employs density functional theory to examine the physicochemical and electronic properties of CHO in both gas and solvent phases. The analysis focuses on molecular optimization, HOMO-LUMO energy gap, density of states, molecular electrostatic potential, vibrational (IR and Raman) and UV-Vis spectra, Mulliken charge distribution, as well as non-covalent interaction (NCI-RDG) and Fukui function analyses.

Methodology

In this study, we conducted different quantum chemical calculations by using the Gaussian16W program (Frisch et al., 2016). The DFT investigations with B3LYP functional (Becke, 1993; Lee et al., 1988a) and 6-311++G (d,p) basis set were used to optimize the geometry and calculate vibrational parameters of the CHO compound. GaussView6.0 (Dennington et al., 2016) was used to visualize the molecule and analyse the findings. The CHO was first optimized for minimum energy at B3LYP/6-311++G (d,p), and it was re-optimized multiple times for accuracy for further calculations. In this study, the B3LYP hybrid functional was employed due to its proven accuracy in predicting the

structural, electronic, and vibrational properties of organic molecules, including oximes. After that, vibrational frequencies were calculated using the earlier optimized structure. The same functional and basis set were used for computing HOMO-LUMO energies, electronic properties, MEP, and DOS spectrum. DOS spectrum of the title compound in the gas phase and in solvents was computed using the GaussSum program (O'Boyle et al., 2008), and vibrational analysis was conducted from the VEDA4 program (Jam-róz, 2013). NCI-RDG analysis was conducted using Multiwfn (Lu and Chen, 2012) and VMD software (Humphrey et al., 1996). Fukui functions were calculated using Gaussian data in the UCA-FUKUI v2.1 software package (Sánchez-Márquez et al., 2014). We applied Koopmans theorem (Koopmans, 1934) for the energy gap which is defined as the difference of the energies of the LUMO and HOMO which eventually leads to other parameters such as Ionization Potential (IP), Electron Affinity (EA), Electronegativity, Chemical potential, Chemical hardness, Chemical softness and Electrophilicity Index (Pearson, 1989; Geerlings et al., 2003; Padmanabhan et al., 2007).

Results and Discussions

Optimized Molecular Geometry:

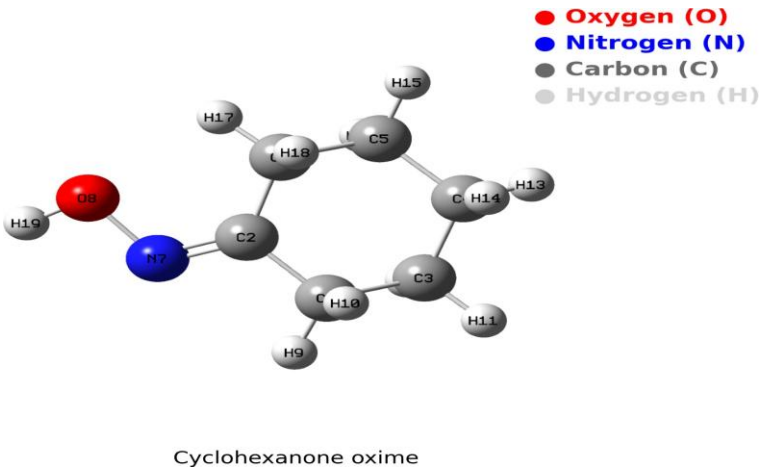

Figure 2: Optimized Structure of CHO with Numbering of Atoms

The optimized geometry of the CHO compound with the minimum energy configuration is computed using Gaussian16W software. Cyclohexanone oxime consists of a six-membered cyclohexane ring, where five of the carbon atoms are each bonded to a pair of hydrogen atoms, while one carbon is substituted with a NOH (oxime) functional group. This substitution alters the electronic and structural properties of the molecule, influencing its vibrational characteristics, which are crucial for spectroscopic analysis. After the optimization process, the molecular structure of cyclohexanone oxime is obtained in its neutral state, providing a reliable foundation for further spectroscopic and computational investigations. The structure of CHO with symbols and labels of atom numbers after optimization in the neutral state is displayed in Figure 2, and different optimized parameters are given in Table 1.

Table 1

Optimized Geometry Parameters and their Calculated Values Using the DFT (B3LYP)/6- 311++G (D,P).

Bond length	Value (Å)	Bond angle	Value	Dihedral angle	Value
C1–C2	1.509	C2–C1–C3	111.078	C3–C1–C2–C6	-50.856
C1–C3	1.541	C1–C3–C4	111.397	C3–C1–C2–N7	127.939
C3–C4	1.535	C3–C4–C5	111.365	H9–C1–C2–C6	-174.573
C4–C5	1.535	C4–C5–C6	112.092	H9–C1–C2–N7	4.222
C5–C6	1.544	C5–C6–C2	110.709	H10–C1–C2–C6	68.591
C2–C6	1.508	C6–C2–C1	116.47	H10–C1–C2–N7	-112.613
C1–H10	1.099	H9–C1–H10	107.438	C2–C1–C3–C4	52.131
C1–H9	1.092	H11–C3–H12	106.736	C2–C1–C3–H11	174.767
C3-H11	1.094	H13–C4–H14	106.511	C2–C1–C3–H12	-63.730
C3–H12	1.097	H15–C5–H16	106.630	H9–C1–C3–C4	174.582
C4–H13	1.095	H17–C6–H18	107.360	H9–C1–C3–H11	-62.782
C4–H14	1.098	H10–C1–C3	108.820	H9–C1–C3–H12	53.721
C5–H15	1.094	H9–C1–C3	111.638	H10–C1–C3–C4	-67.005
C5–H16	1.096	H10–C1–C2	108.300	H10–C1–C3–H11	55.630
C6–H17	1.089	H11–C3–C1	109.590	H10–C1–C3–H12	172.133
C6–H18	1.098	H11–C3–C4	110.531	C1–C2–C6–C5	50.102
C2–N7	1.277	H12–C3–C4	109.413	C1–C2–C6–H17	173.874
N7–O8	1.418	H12–C3–C1	109.047	C1–C2–C6–H18	-69.061
O8–H19	0.962	H9–C1–C2	109.437	N7–C2–C6–C5	-128.554
		H13–C4–C3	110.138	N7–C2–C6–H17	-4.783
		H13–C4–C5	110.003	N7–C2–C6–H18	112.282
		H14–C4–C3	109.321	C1–C2–N7–O8	179.887
		H14–C4–C5	109.374	C6–C2–N7–O8	-1.458
		H15–C5–C4	110.490	C1–C3–C4–C5	-55.649
		H15–C5–C6	109.298	C1–C3–C4–H13	-177.973
		H16–C5–C4	109.310	C1–C3–C4–H14	65.324
		H16–C5–C6	108.855	H11–C3–C4–C5	-177.743
		H17–C6–C5	111.268	H11-C3–C4–H13	59.933
		H17–C6–C2	110.549	H11–C3–C4–H14	-56.769
		H18–C6–C5	109.021	H12–C3–C4–C5	64.996
		H18–C6–C2	107.96	H12-C3–C4–H13	-57.327
		C6–C2–N7	126.788	H12–C3–C4–H14	-174.029
		C1–C2–N7	116.720	C3–C4–C5–C6	55.435
		C2–N7–O8	112.789	C3–C4–C5–H15	177.606
		N7–O8–H19	102.083	C3–C4–C5–H16	-65.349
				H13–C4–C5–C6	177.836
				H13–C4–C5–H15	-59.992
				H13–C4–C5–H16	57.052
				H14–C4–C5–C6	-65.507
				H14–C4–C5–H15	56.663

Bond length	Value (Å)	Bond angle	Value	Dihedral angle	Value
				H14–C4–C5–H16	173.707
				C4–C5–C6–C2	-51.193
				C4–C5–C6–H17	-174.551
				C4–C5–C6–H18	67.228
				H15–C5–C6–C2	-174.042
				H15–C5–C6–H17	62.6003
				H15–C5–C6–H18	-55.621
				H16–C5–C6–C2	69.853
				H16–C5–C6–H17	-53.504
6				H16–C5–C6–H18	-171.725
				C2–N7–O8–H19	179.278

Global Reactivity Descriptors

Table 2

Global Reactivity Descriptors of the Cyclohexanone Oxime Molecule in the Gas Phase and Different Solvents

Parameters	gas phase	solvent water	solvent DMSO	solvent ethanol
Total Energy (eV)	-9934.50	-9934.51	-9934.52	-9934.51
Dipole (Debye)	1.28	1.95	1.95	1.93
HOMO (E_{HOMO}) (eV)	-6.91	-7.12	-7.11	-7.11
LUMO (E_{LUMO}) (eV)	-0.46	-0.45	-0.45	-0.45
Energy gap (eV)	6.45	6.67	6.66	6.66
Ionization Potential (IP) (eV)	6.91	7.12	7.11	7.11
Electron Affinity (EA) (eV)	0.46	0.45	0.45	0.45
Electronegativity (χ)(eV)	3.68	3.79	3.78	3.78
Chemical potential (μ)(eV)	-3.68	-3.78	-3.78	-3.78
Chemical hardness (η)(eV)	3.22	3.34	3.33	3.33
Chemical softness (S)$(eV)^{-1}$	0.16	0.15	0.15	0.15
Electrophilicity index (ω)(eV)	2.11	2.13	2.14	2.14

All the calculated values of different global reactivity descriptors are listed in Table 2. These calculations show that HOMO energy values change from -6.91 eV in the gas phase to around -7.11 eV in different solvents, whereas LUMO energies remain unchanged at around -0.45 eV. The energy gap increases in solvents, meaning that CHO is more stable in solvents than in the gas phase. Ionization Potential increases in solvents, indicating more energy is required to remove an electron, implying greater stability in solvents, whereas Electron affinity remains nearly constant, suggesting minimal effects of solvent on electron accepting ability. Electronegativity increases in solvents (gas phase:3.68 eV to solvents:3.78 eV), indicating a stronger tendency to attract electrons in solution. Chemical potential is lower in solvents, reflecting greater stability. Hardness increases slightly in solvents, indicating higher resistance to electronic deformation. Chemical softness decreases slightly

in solvents, meaning reduced reactivity. According to the global electrophilicity index (Domingo et al., 2016), carbon-based compounds can be classified into three different categories as weak electrophiles ($\omega < 0.8$ eV), moderate electrophiles (0.8 eV $< \omega < 1.5$ eV), and powerful electrophiles ($\omega > 1.5$ eV). From this research, we understand that CHO has strong electrophilicity in the gas phase as well as in solvents. Additionally, electrophilicity is slightly higher in solvents, indicating a higher tendency to accept electrons in solution.

Frontier Molecular Orbitals (FMO) Study:

The Highest Occupied Molecular Orbital (HOMO) and the Lowest Unoccupied Molecular Orbital (LUMO) are the Frontier Molecular Orbitals (FMOs) as they are present at the outermost boundaries and are very important parameters to conduct various quantum chemical calculations. HOMO acts as the capacity to donate an electron, i.e., a nucleophile, whereas LUMO acts as the capacity to gain an electron, i.e., an electrophile (Janani et al., 2021; Mamand, 2019). The energy gap, which is given by the difference in LUMO and HOMO energy, has been considered to be an indicator of chemical reactivity, kinetic stability, and polarizability of the compound (Rijal et al., 2022; Dege et al., 2022; Khanal et al., 2025). The FMOs of the CHO molecule are computed in gas phase as well as in solvents water, DMSO, and ethanol, by using the B3LYP functional along with the 6-311++G (d,p) basis set, as shown in Figure 3.

The red and green colors in the FMOs symbolize the negative and positive regions accurately. The more the value of the energy gap, more the kinetic stability and the less the chemical reactivity of the compound (Hussain et al., 2020). The HOMO and LUMO energies of CHO in the gas phase and solvent media are as mentioned in Table 2. The cyclohexanone oxime compound shows a higher energy gap in solvent phases (6.66eV) than in the gas phase (6.45 eV), symbolizing the lowest chemical reactivity and highest kinetic stability in solvent phases. From Figure 2, the HOMO is more localized towards the oxime group and carbons near it, while the LUMO is completely localized in the cyclohexane ring and very little towards the oxime group.

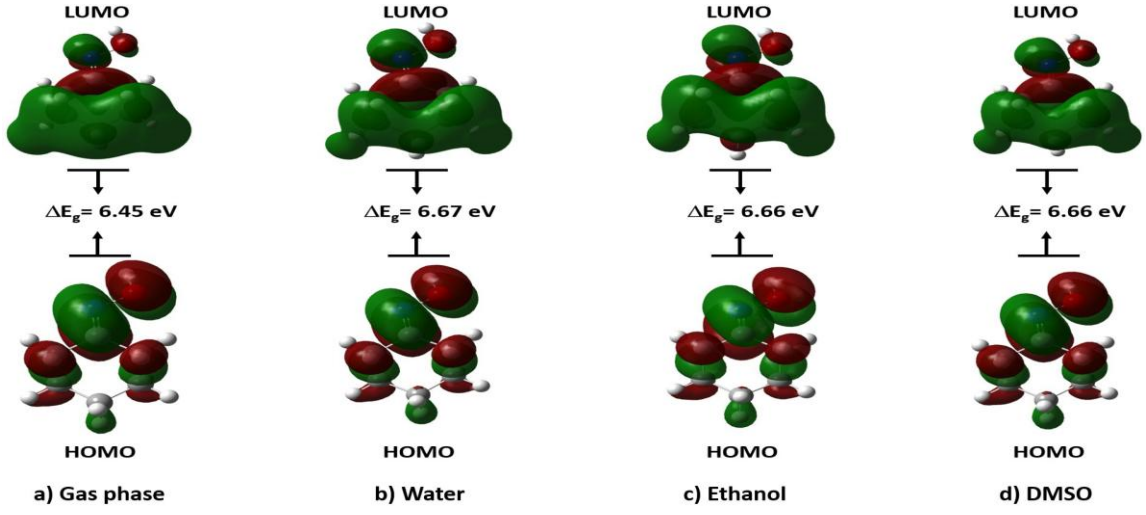

Figure 3: Frontier Molecular Orbitals of Cyclohexanone Oxime in Neutral State

Thermochemistry:

Various parameters obtained from Gaussian calculations relating different thermodynamic functions like thermal energy, heat capacity, and entropy are presented in Table 3. These calculations show that total thermal energy, heat capacity, and entropy are predominantly influenced by vibrational contributions. Translational and rotational motions provide equal thermal energies and heat capacities, but their entropy contributions are significant at 40.085 and 28.262 cal/mol-K, respectively. The electronic contribution is zero, which is as expected because we calculated these parameters in the ground state.

Table 3

Thermochemistry of Cyclohexanone Oxime in Neutral State

	Thermal Energy (kcal/mol)	Heat Capacity (cal/mol-Kelvin)	Entropy (cal/mol-Kelvin)
Total	109.649	29.941	85.107
Electronic	0.000	0.000	0.000
Translational	0.889	2.981	40.085
Rotational	0.889	2.981	28.262
Vibrational	107.871	23.980	16.760

Density Of States (DOS) Spectra:

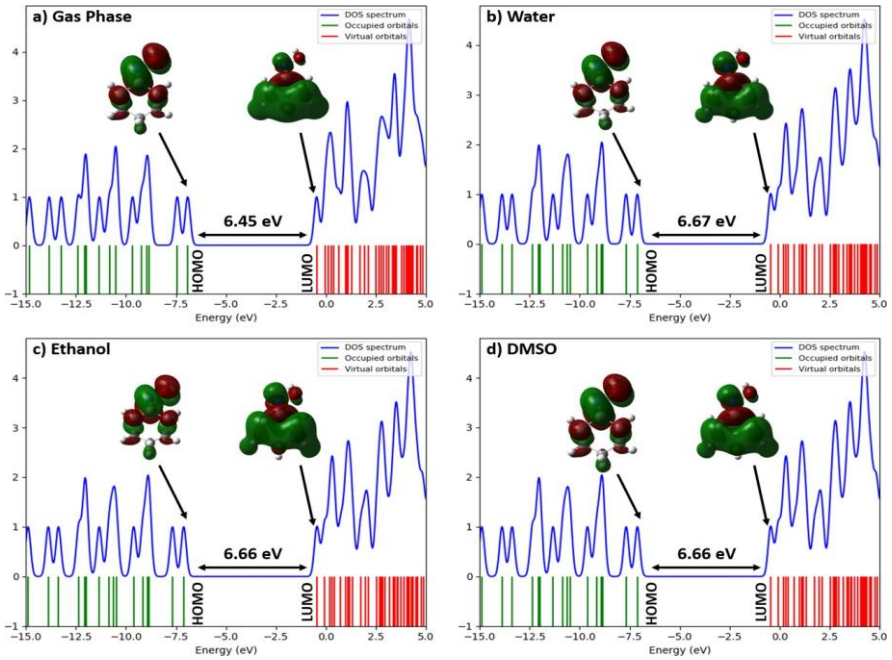

Figure 4: DOS Spectra of Cyclohexanone Oxime in Gas Phase and Different Solvent Media

The density of states (DOS) spectrum explains the energy level per unit energy increase. Hence, higher Density Of States (DOS) means more accessibility for the states to be occupied at a given energy level (Ben Mahmoud et al., 2020; Pandey et al., 2011). The red lines in the DOS spectrum symbolize the LUMO, whereas green lines symbolize the HOMO energy levels. The DOS spectra of

the cyclohexanone oxime compound, including several states with different energy levels in the neutral state in the gas phase and different solvents within the energy range of -15 eV to +5 eV, are illustrated in Figure 4. From these spectra, the energy difference in LUMO and HOMO, i.e., the energy gap in the gas phase, is found to be 6.45eV, whereas in solvents it is calculated to be about 6.66eV. This also shows a higher energy gap in solvents than in the gas phase. These values from DOS spectrum are in strong agreement with the values from FMOs above.

Mulliken Atomic Charge Distribution:

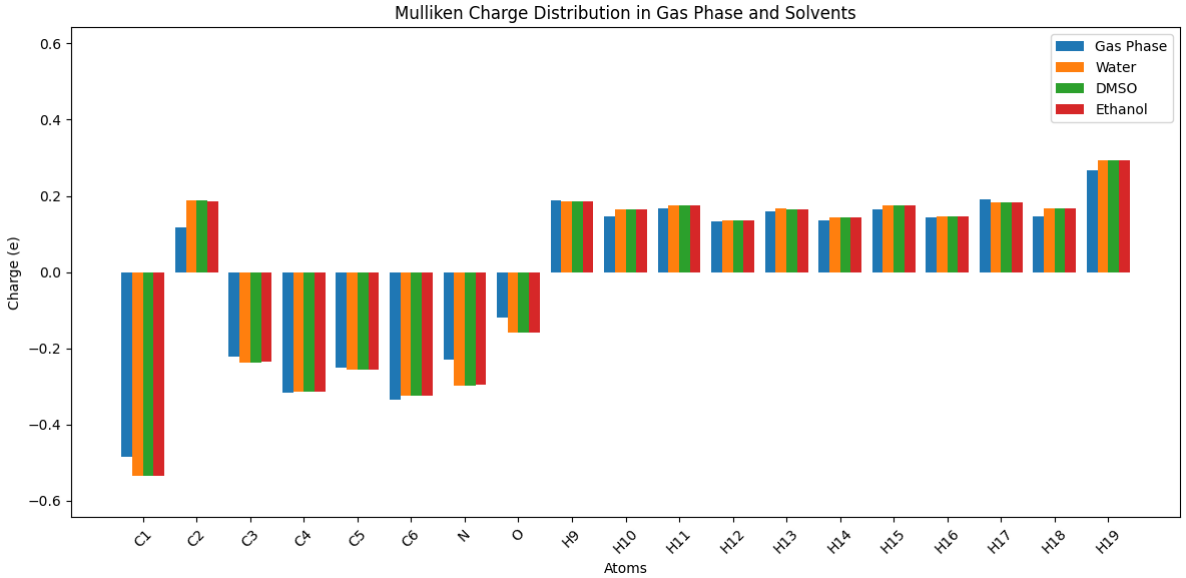

Figure 5: Mulliken Atomic Charge Distribution plot of CHO

In various quantum chemical calculations, Mulliken atomic charges have a very strong impact on the electronic structures, molecular properties, polarizability, dipole moment, and many other properties (Mulliken, 1955; Kamal et al., 2025; Gyawali et al., 2025). The Mulliken atomic charges of the cyclohexanone oxime compound in the gas phase and different solvents are listed in Table 4, and a plot of atoms with their Mulliken atomic charges is illustrated in Figure 5. From the calculations, we get to know that every other carbon atoms have negative Mulliken charge, but C2 has a positive Mulliken charge. This might be because it likely experiences electron withdrawal from nearby electronegative atoms like N or O, as this carbon atom is connected to the oxime group. Due to bonding, resonance, and hybridization effects. This makes C2 electron-deficient, while other carbons retain more electron density, leading to negative charges.

Table 4

Mulliken Charge Distribution in Gas Phase and Different Solvents

Atom	Gas Phase	Water	DMSO	Ethanol
C1	-0.485239	-0.535109	-0.534614	-0.533530
C2	0.117910	0.187967	0.187277	0.185768
C3	-0.222946	-0.236403	-0.236290	-0.236039
C4	-0.315853	-0.315008	-0.315008	-0.315009

Atom	Gas Phase	Water	DMSO	Ethanol
C5	-0.251623	-0.256584	-0.256557	-0.256497
C6	-0.335314	-0.323866	-0.323991	-0.324265
N	-0.229013	-0.297391	-0.296676	-0.295115
O	-0.119502	-0.158697	-0.158326	-0.157514
H9	0.188990	0.184514	0.184588	0.184746
H10	0.145430	0.164045	0.163837	0.163383
H11	0.166391	0.175561	0.175455	0.175226
H12	0.132818	0.136413	0.136396	0.136355
H13	0.159197	0.166000	0.165928	0.165770
H14	0.135923	0.143213	0.143120	0.142918
H15	0.165358	0.175079	0.174970	0.174731
H16	0.143881	0.146901	0.146890	0.146863
H17	0.189770	0.182721	0.182813	0.183012
H18	0.145975	0.166752	0.166524	0.166027
H19	0.267846	0.293894	0.293667	0.293168

Molecular Electrostatic Potential (MEP) Analysis:

MEP is a very important tool for studying and examining molecular structure and different physicochemical parameters along with their relationship with several drugs and biological compounds (Khadka et al., 2025; Murray and Sen, 1996; Alkorta and Perez, 1991). MEP is employed in order to map the distribution of electrons in molecules and for distinguishing electrophilic and nucleophilic sites (Khanal et al., 2025). From Figure 6, the plot of MEP of CHO compound in neutral state illustrates the classified order of surface region is blue > green > yellow > orange > red where blue region represents the region with most positive electrostatic potential while the red region represents the region with most negative electrostatic potential and green regions represents the regions with zero electrostatic potential (Dhurjad et al., 2025). In the cyclohexanone oxime molecule, electrostatic potential lies in between -4.564e-2 a.u to +4.564e-2 a.u (gas phase), -4.636e-2 a.u to +4.636e-2 a.u (ethanol), -4.634e-2 a.u to +4.634e-2 a.u (water), and -4.635e-2 a.u to +4.635e-2 a.u (DMSO). The region around the NOH (oxime) group is covered by orange to red regions, which symbolize that this region is prone to electrophilic attack. The red regions are darker in solvent phases than in the gas phase, indicating that their effect is more pronounced in solvents compared to in the gas phase. The regions around the cyclohexane ring, except C2, appear green, indicating zero electrostatic potential in that region. The region above the hydrogen atom attached to the oxygen atom appears to be blue, which indicates it might be prone to nucleophilic attack. The regions around the cyclohexane ring, except C2, appear green, indicating zero electrostatic potential in that region.

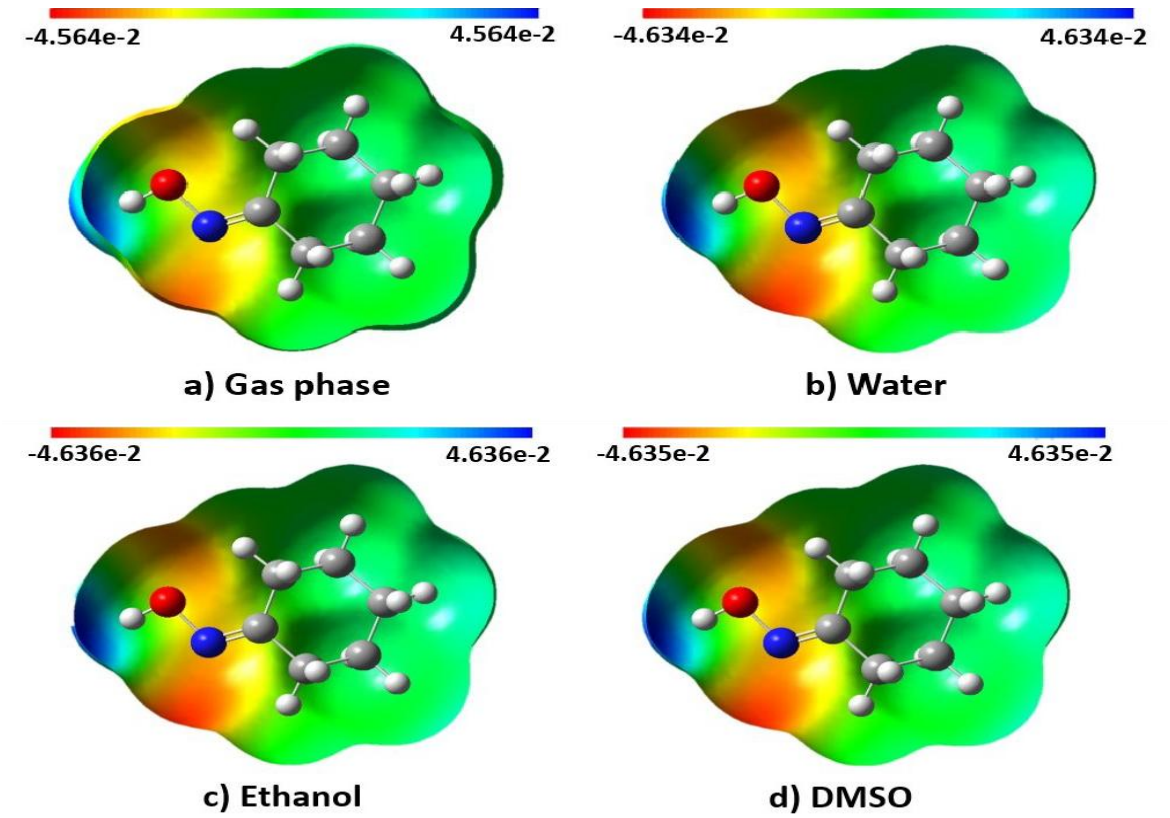

Figure 6: MEP of CHO in neutral state in gas phase and different solvents

NCI-RDG Analysis

The NCI-RDG (Non-Covalent Interaction - Reduced Density Gradient) method allows researchers to study various intermolecular interactions deeply by distinguishing between van der Waals forces and steric repulsion, and hydrogen bonds in molecules. RDG is a fundamental dimensionless quantity that characterizes weak interactions based on the quantum-mechanical electron density and its first derivatives in real space (Johnson et al., 2010).

In the NCI-RDG evaluation of cyclohexanone oxime, both the steric hindrance and the Van der Waals attractive forces are observed. From the RDG analysis, it is shown in Figure 7 (a and b), the blue regions in the RDG vs. sign $(\lambda_2)\rho$ scatter plot (between 0.03 and 0.05 a.u.) correspond to strong attractive interactions, such as hydrogen bonding. This is also visualized in the isosurface plot near the oxime functional group, particularly between the oxime OH hydrogen and the nitrogen. The green regions (sign $(\lambda_2)\rho$ between 0.02 and 0.01 a.u.) signify weak van der Waals interactions, commonly seen between non-bonded atoms in close convergence, especially around the cyclohexane ring and adjacent atoms. The red spikes in the plot (sign $(\lambda_2)\rho$ >0.01 a.u.) indicate steric repulsion, visualized in the isosurface diagram near the ring hydrogens and oxygen atom. This suggests electron cloud overlap and steric hindrance in these regions. This information is also supported by the RDG isosurface mapping, which reveals that steric hindrance exists as red regions inside the ring, while weak Van der Waals interactions appear as green regions.

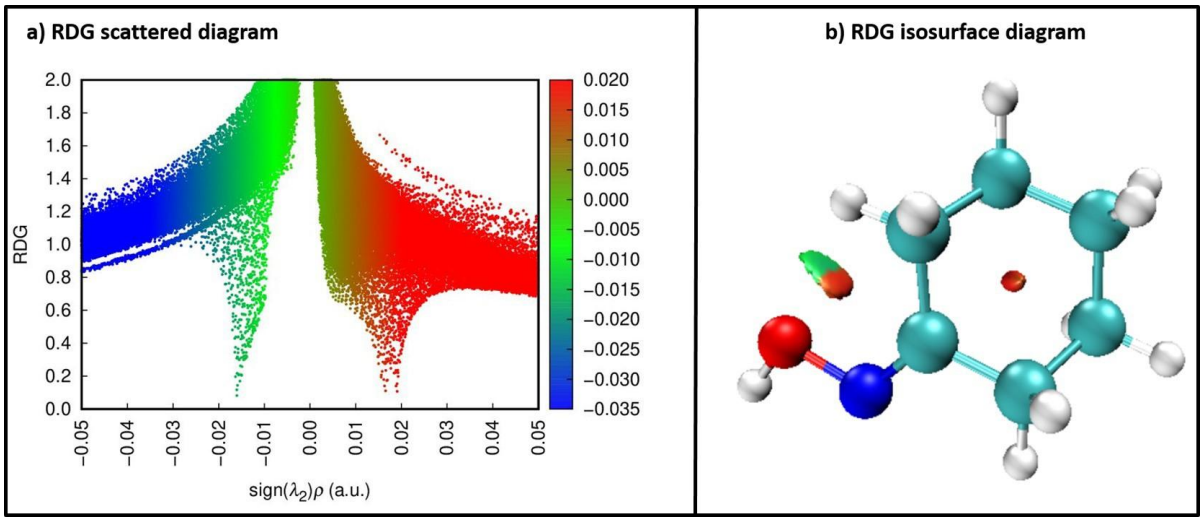

Figure 7: Reduced density gradient (RDG) analysis and NCI (a) 2D and (b) 3D

UV-Vis Absorption Spectra:

It is known that the availability of electrons greatly affects the maximum UV wavelength absorption (Saji et al., 2021). The UV-Vis absorption spectra of the cyclohexanone oxime molecule were obtained after the calculation with TD-DFT with B3LYP functional using 6- 311++G (d,p) basis set in neutral state in gas phase as well as in different solvents like water, DMSO, and ethanol. Different parameters like oscillatory strength, excitation energies, and maximum wavelength, along with major contributions of the cyclohexanone oxime compound, are given in Table 5. The UV-Vis absorption spectra are displayed in Figure 8. From the spectra, we observe that the absorption of UV wavelengths in the spectrum is hugely affected by the polarity of different solvents like water, ethanol, and DMSO used compared to the gas phase.

Table 5

UV-Vis Absorption Excitation Energy and Oscillator Strength with Maximum Wave-length and Major Contributions

State	Maximum Wavelength (nm)	Excitation Energy (eV)	Oscillator strength (f)	Major Contributions
Gas Phase	213	5.82	0.0210	(H → L (45%), (H → L+1 (36%), (H-1 → L (11%)
	211	5.88	0.0055	(H-1 → L (62%), (H-1 → L+4 (11%)
	205	6.04	0.0699	(H → L (44%), (H → L+1 (42%)
Water	208	5.97	0.0219	(H-1 → L (49%), (H → L (19%), (H → L+1 (19%)
	206	6.02	0.0210	(H-1 → L (32%), (H → L (23%), (H → L+1 (34%)
	198	6.25	0.1792	(H → L (52%), (H → L+1 (35%)
Ethanol	208	5.96	0.0138	(H-1 → L (48%), (H → L (20%), (H → L+1 (20%)
	206	6.02	0.0219	(H → L (24%), (H-1 → L (32%), (H → L+1 (33%)
	199	6.24	0.1785	(H → L (51%), (H → L+1 (36%)
DMSO	208	5.96	0.0144	(H-1 → L (48%), (H → L (20%), (H → L+1 (20%)
	206	6.02	0.0230	(H-1 → L (32%), (H → L (24%), (H → L+1 (33%)

State	Maximum Wavelength (nm)	Excitation Energy (eV)	Oscillator strength (f)	Major Contributions
	199	6.24	0.1863	(H → L (51%), (H → L+1 (37%)

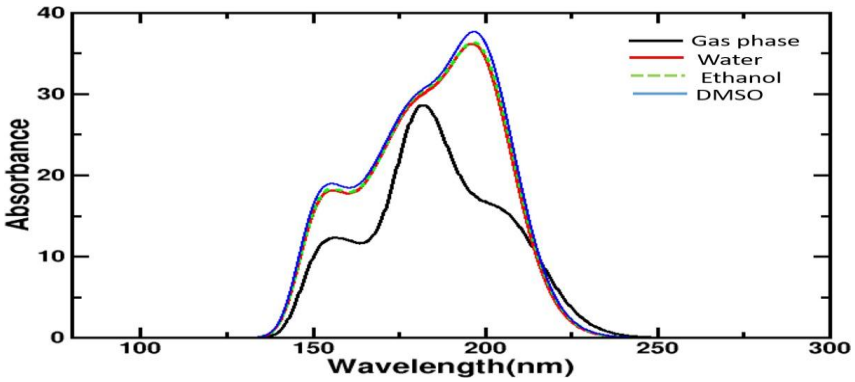

Figure 8: UV-Vis Spectra of Cyclohexanone Oxime in Gas Phase And Different Solvents

Vibrational Analysis:

Cyclohexanone oxime has 19 atoms with 51 theoretical modes of vibrations. We performed frequency calculation analysis after complete optimization of the molecule to a minimum energy multiple times in the gas phase, which is confirmed by the absence of negative frequencies. Table 6 shows the calculated values of vibrational frequencies, their IR intensities, Raman activities, and vibrational assignments along with their potential energy distribution (PED%) contributions in the gas phase. The wavenumber linear scaling method was used for uniform scaling of calculated vibrational frequencies for the DFT with B3LYP functional and 6-311++G (d,p) basis set whose formula is given as: $\nu_{observed} = \nu_{calculated} \times (1.0087 - 0.0000163\,\nu_{calculated})$ (Yoshida et al., 2000). FT-Raman spectrum and FT-IR spectrum are illustrated in Figure 9 (a) and 9 (b), respectively.

In FT-IR spectra of cyclohexanone oxime strongest band was observed at wavenumber 2994 (2874-scaled) corresponding to [C1-H10] and [C6-H18] with 81% and 10% as their PED contributions, respectively. And a medium band was observed at wavenumber 3123 (2991-scaled), which corresponds to[C6-H17] with 97% PED contribution. Similarly, some weak bands were also observed at wavenumbers 3842 (3635-scaled) and 1721 (1688-scaled) corresponding to vibrations [O8-H19] (100% PED) and [N7-C2] (78% PED) respectively. And in FT-Raman spectra, strongest Raman band was observed at wavenumber 3123 (2991-scaled) corresponding to vibration [C6-H17] (97% PED) and some medium to weak bands were observed at wavenumbers 2994 (2878-scaled), 1402 (1382-scaled), 869 (864-scaled) and 398 (399-scaled) corresponding to C-H stretching vibration, bending H-C-H vibrations, torsional ring carbon vibrations and bending C-C-C vibrations respectively.

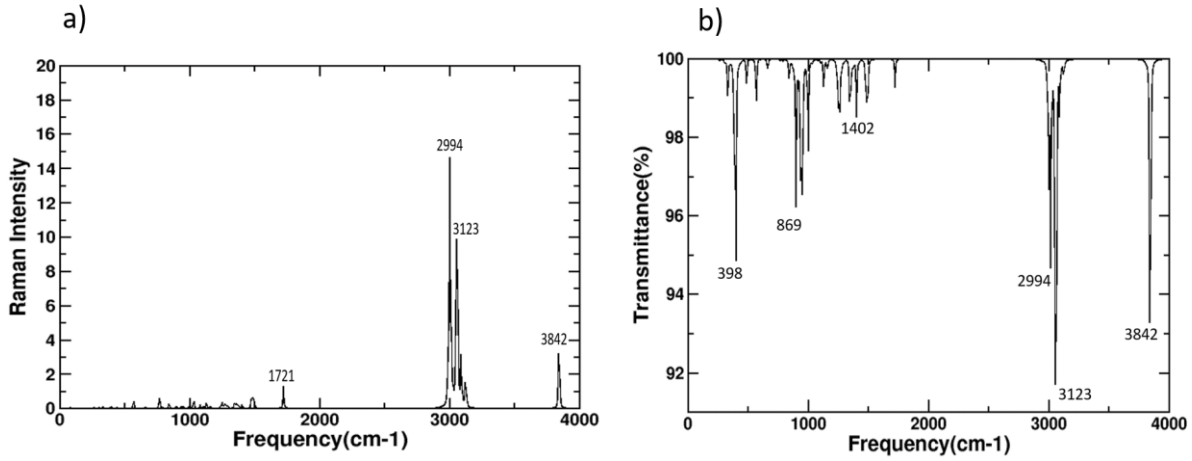

Figure 9: Theoretical (a) FT-Raman and (b) FT-IR Spectra of cyclohexanone oxime

C-H vibrations: Typical C-H stretching modes of vibrations are observed in the range just lower than 3000 cm^{-1} (Eggers and Lingren, 1956; Kemp, 1991). In our study, the FT- IR frequency of C-H stretching vibration was found at 2991 and 2874 cm^{-1} in the gas phase with PED contributions of 97 and 91, respectively, which is in very close agreement with the above-mentioned literature.

O-H Vibrations: Usually, the stretching frequency for O-H for oximes utilizing non-polar solvents in a dilute solution are observed in the range of 3570-3650 cm^{-1} while it is observed in the range of 3130-3300 cm^{-1} in the presence of hydrogen bonding (St and Flett, 1957; Karabacak et al., 2010). In our study, we observed this vibration at 3635 cm^{-1}, which is also in close match to other experimental studies.

C=N Vibrations: In our research, C=N vibrations are observed at 1721 $cm^{-1,}$ which is a little higher value to the usual C=N stretching vibration, which is commonly observed in the range of 1620-1690 cm^{-1} in various oximes (Fabian et al., 1956; Hadi, 1956).

Table 6

Vibrational Analysis of CHO With its Vibrational Frequencies, IR Intensities, Raman Activities, and Assignments Along with Potential Energy Distribution in The Gas Phase

Calculated Frequency (cm-1)		IR	Raman	Vibrational assignments
Unscaled	Scaled	Intensity	Activity	[PED>10%]
3842	3635	106.51	137.16	ν[*O*8 −*H*19](100)
3123	2991	6.32	62.50	ν[*C*6 −*H*17](97)
2994	2874	10.64	62.27	ν[*C*1 −*H*10](81), ν[*C*6 −*H*18](10)
1721	1688	9.67	26.89	ν[*N*7 −*C*2](78)
1505	1481	0.73	1.27	β[*H*9 −*C*1 −*H*10](89)
1402	1382	22.49	5.13	β[*H*19 −*O*9 −*N*7](40), β[*H*17 −*C*6 −*C*2](16)
1157	1145	4.35	2.16	β[*H*15 −*C*5 −*C*6](43), τ[*H*16 −*C*5 −*C*6 −*C*2](13)
1079	1069	0.26	4.05	ν[*C*3 −*C*4](61)

				$\beta[H13-C4-C5](13),\tau[H13-C4-C5-C6](28),$ $\tau[C1-C3-C4-C5](25)$ $\beta[C1-C3-C4](16),\beta[C6-C2-N7](14),$ $\tau[H18-C6-C2-C1](13),\tau[C3-C1-C2-C6](11)$ $\beta[C3-C4-C5](31),\tau[H9-C1-C2-C6](18),$ $\tau[H15-C5-C6-C2](14)$ $\tau[H19-O9-N7-C2](50),\beta[C3-C4-C5](12),$ $\beta[C1-C2-C6](15)$ $\beta[C6-C2-N7](30),\beta[C2-C1-C3](10),$ $\tau[C1-C3-C4-C5](10),\tau[C1-C2-N7-O8](17)$ $\beta[C2-N7-O8](10),\tau[C3-C1-C2-C6](10),$ $\tau[C2-C1-C3-C4](44)$
81	82	0.02	0.94	$\gamma[N7-C1-C6-C2](64)$

ν = stretching vibrations, β = Bending vibrations, τ = Torsional vibrations, γ = Out vibrations

Fukui function:

The Fukui functions were calculated using Gaussian output data in UCA-FUKUI v2.1 software and are listed in Table 7. The Fukui function is the most important local reactivity descriptor. This gives the most favourable sites in a molecule for electron redistribution when the electron count varies. Fukui functions also indicate the tendency of electron density to shift at specific points upon electron donation or acceptance (Lee et al., 1988b; Khadka et al., 2025).

The Fukui function analysis for CHO reveals that Oxygen at site 8 (f^-=0.2603) is the most nucleophilic site, mainly because of the presence of lone pairs. So, this site is highly reactive towards electrophilic attacks. Also, Carbon at site 2 (f^-=0.2151) and Nitrogen at site 7 (f^-=0.1447) also show notable nucleophilic nature. Hydrogen atoms at sites 14 (f^+ =0.1369), site 13 (f^+=0.1234), and site 19 (f^+=0.1221) are the most electrophilic sites, indicating a preferred site for nucleophilic attacks or hydrogen bonding interactions. The overall reactivity descriptor (f^0) further confirms that the Oxygen at site 8 (f^0=0.143), Carbon at site 2 (f^0=0.1086), and nitrogen at site 7 (f^0=0.0874) are the main reactive centers of the CHO molecule.

Table 7

Fukui Function Values for Different Atomic Sites

Atoms		**Sites**	$\mathbf{f^-}$	$\mathbf{f^+}$	$\mathbf{f^0}$
	C	1	-0.0299	0.0063	0.0118
	C	2	0.2151	0.0021	0.1086
	C	3	0.0099	0.0158	0.0129
	C	4	-0.0093	0.0310	0.0108
	C	5	0.0061	0.0179	0.0120
	C	6	-0.0206	0.0075	0.0066
	N	7	0.1447	0.0301	0.0874
	O	8	0.2603	0.0256	0.1430

Atoms		Sites	f^-	f^+	f^0
	H	9	0.0290	0.0353	0.0322
	H	10	0.0726	0.0670	0.0698
	H	11	0.0433	0.1049	0.0741
	H	12	0.0232	0.0331	0.0281
	H	13	0.0492	0.1234	0.0863
	H	14	0.0219	0.1363	0.0791
	H	15	0.0399	0.1001	0.0700
	H	16	0.0204	0.0365	0.0284
	H	17	0.0156	0.0381	0.0268
	H	18	0.0637	0.0667	0.0652
	H	19	0.0450	0.1221	0.0836

Conclusion

In this study, we explored the structure, properties, and spectroscopic analysis of cyclohexanone oxime using quantum mechanical calculations. We employed a common method in computational physics known as Density Functional Theory (DFT), specifically the B3LYP functional, along with the 6-311++G (d,p) basis set, which enables the accurate description of electron behavior in molecules. First, we optimized the shape (geometry) of the molecule multiple times in the gas phase to find its most stable form, that is, the form with the lowest energy. After confirming the stability, we calculated the vibrational frequencies to better understand how the molecule behaves under different conditions. We then studied the molecules Frontier Molecular Orbitals (HOMO and LUMO) and found that the energy gap between them is larger in solvents compared to the gas phase. This suggests that cyclohexanone oxime becomes more stable when surrounded by a solvent, which was further supported by Density of States (DOS) spectra analysis.

When we looked at the FT-IR (Infrared) spectrum, we identified strong polar vibrations like the stretching of OH and C=N bonds. In contrast, the FT-Raman spectrum highlighted non-polar vibrations such as CC bond stretches. These findings help explain how different parts of the molecule move or vibrate when exposed to light or energy. The UV-Visible (UV-Vis) analysis showed that the molecule absorbs more ultraviolet light when in a solvent than in the gas phase. This supports the idea that solvents influence the electronic properties of the molecule. Using Non-Covalent Interaction (NCI) and Reduced Density Gradient (RDG) analysis, we found that strong hydrogen bonding occurs between atoms in the oxime group, which is an important feature in its chemical behavior. Additionally, the Molecular Electrostatic Potential (MEP) map and Fukui function analysis helped us pinpoint the most reactive parts of the molecule. Oxygen was found to be the most electron-rich (nucleophilic) site, followed by the carbon and nitrogen atoms in the oxime group. Overall, the theoretical results we obtained closely matched the past experimental observations and agreed well

with findings from other scientific studies. This confirms the reliability of our computational approach in understanding the molecular behavior of cyclohexanone oxime.

Conflict of Interest

The authors declare that there are no conflict of interest related to this work.

Data Availability

The data supporting the findings of this study are available within the article. Additional datasets can be made available by the corresponding author upon reasonable request.

Acknowledgments

The authors thank Prof. Dr. Rajendra Parajuli and Asst. Prof. Pitambar Shrestha of Amrit College (ASCOL), TU, Kathmandu, Nepal, for providing access to Gaussian calculation.

References

Alkorta, I., & Perez, J. J. (1996). Molecular polarization potential maps of the nucleic acid bases. *International Journal of Quantum Chemistry*, *57*(1), 123-135.

Becke, A. D. (1993). Density-functional thermochemistry. iii. the role of exact exchange. *The Journal of Chemical Physics*, 98:5648–5652.

Ben Mahmoud, C., Anelli, A., Csányi, G., and Ceriotti, M. (2020). Learning the electronic density of states in condensed matter. *Physical Review B*, 102(23):235130.
Chemical Reviews, 103:1793–1874.

Dege, N., Gökce, H., Doan, O. E., Alpaslan, G., Aar, T., Muthu, S., and Sert, Y. (2022). Quantum computational, spectroscopic investigations on n-(2-((2-chloro-4,5- dicyanophenyl) amino)ethyl)-4-methylbenzenesulfonamide by DFT/TD-DFT with different solvents, molecular docking and drug-likeness researches. *Colloids and Surfaces A: Physicochemical and Engineering Aspects*, 638:128311.

Dennington, R., Keith, T. A., and Millam, J. M. (2016). *GaussView, Version 6*. Semichem Inc., Shawnee Mission, KS.

Dhurjad, C., Sharma, S., Shinde, R. A., Alzahrani, A. Y. A., & Adole, V. A. (2025). Synthesis, Computational and Biological Evaluation of Imidazole Pyrazole Hydrazones as Antitubercular Agents. *Journal of Molecular Structure*, 144667.

Domingo, L. R., Ríos-Gutiérrez, M., and Pérez, P. (2016). Applications of the conceptual density functional theory indices to organic chemistry reactivity. *Molecules*, 21:748.

Eggers, D. F. and Lingren, W. E. (1956). C–H vibrations in aldehydes. *Analytical Chemistry*, 28(8):1328–1329. Elsevier, Amsterdam.

Fabian, J., Goutarel, R., and Goutarel, M. (1956). Synthèse et propriétés des dérivés de la 2,3-dihydro-1H-pyrrolo[3,4-b]quinolin-1-one. *Bulletin de la Société Chimique de France*, 1956(10):1499–1504.

Fisher, W. B. and Cresentini, L. (1985). Caprolactam. In *Kirk-Othmer Concise Encyclopedia of Chemical Technology*, page 920. John Wiley and Sons, New York.

Frisch, M. J., Trucks, G. W., Schlegel, H. B., Scuseria, G. E., Robb, M. A., Cheeseman, J. R., and et al. (2016). *Gaussian 16, Revision C.01*. Gaussian, Inc., Wallingford, CT.

Geerlings, P., Proft, F. D., and Langenaeker, W. (2003). Conceptual density functional theory.

Gyawali, K., Chhetri, S., Khanal, K., Kshetri, M., Maharjan, R., Acharya, A., Khanal, M., Ghimire, M., and Lamichhane, T. (2025). Inhibition potential of quercetin similar compounds to SARS-CoV-2 main protease by high-throughput virtual screening, molecular simulations, ADMET analysis, and DFT studies. *Chemistry & Biodiversity*, page e01485.

Hadi, D. (1956). Infrared spectra and structure of some quinone monoximes. *Journal of the Chemical Society (Resumed)*, pages 2725–2731.

Humphrey, W., Dalke, A., and Schulten, K. (1996). VMD - visual molecular dynamics. *Journal of Molecular Graphics*, 14:33–38.

Hussain, R., Saeed, M., Mehboob, M. Y., Khan, S. U., Khan, M. U., Adnan, M., and Ayub,

Jamróz, M. H. (2013). Vibrational energy distribution analysis (VEDA): Scopes and limitations.

Janani, S., Rajagopal, H., Muthu, S., Aayisha, S., Raja, M., and Irfan, A. (2021). Structural, vibrational, electronic properties, hirshfeld surface analysis topological and molecular docking studies of n-[2-(diethylamino) ethyl]-2-methoxy-5-methylsulfonylbenzamide. *Heliyon*, 7(10).

Johnson, E. R., Keinan, S., Mori-Sánchez, P., Contreras-García, J., Cohen, A. J., and Yang,

K. (2020). Density functional theory study of palladium cluster adsorption on a graphene support. *RSC Advances*, 10(35):20595–20607.

Karabacak, M., Cinar, M., Unal, Z., and Kurt, M. (2010). FT-IR, UV spectroscopic and DFT quantum chemical study on the molecular conformation, vibrational and electronic transitions of 2-aminoterephthalic acid. *Journal of Molecular Structure*, 982(1-3):22–27.

Kemp, W. (1991). *Organic Spectroscopy*. Macmillan Press Ltd., London.

Khadka, M., Sah, M., Chaudhary, R., et al. (2025). Spectroscopic, quantum chemical, and topological calculations of the phenylephrine molecule using density functional theory. *Scientific Reports*, 15:208.

Khanal, K., Kshetri, M. B., Ghimire, M. P., & Lamichhane, T. R. (2025). *In silico* study on structural, electronic, and adsorption properties of cisplatin/(TiO_2) n (n= 2–5) nanoclusters and interactions with hen egg white lysozyme. *Materials Research Express*, *12*(11), 115001.

Khanal, K., Kshetri, M. B., Khanal, M., Acharya, A., Maharjan, R., Gyawali, K., Ghimire,

Koopmans, T. (1934). Über die zuordnung von wellenfunktionen und eigenwerten zu den einzelnen elektronen eines atoms. *Physica*, 1:104–113.

Kozyro, A. A., Kabo, G. J., Krouk, V. S., Sheiman, M. S., Yursha, I. A., Simirsky, V. V., Krasulin, A. P., Sevruk, V. M., and Gogolinsky, V. I. (1992). Thermodynamic properties of cyclohexanone oxime. *The Journal of Chemical Thermodynamics*, 24(8):883–895.

Lee, C., Yang, W., and Parr, R. G. (1988a). Development of the colle-salvetti correlation-energy formula into a functional of the electron density. *Physical Review B*, 37:785–789.

Lee, C., Yang, W., and Parr, R. G. (1988b). Local softness and chemical reactivity in the molecules CO, SCN^- and H2CO. *Journal of Molecular Structure: Theochem*, 163:305–313.

Lide, D. R., editor (1992). *Handbook of Chemistry and Physics*. CRC Press, Boca Raton, FL, 73rd edition.

Lu, T. and Chen, F. (2012). Multiwfn: A multifunctional wavefunction analyzer. *Journal of Computational Chemistry*, 33:580–592.

M. P., and Lamichhane, T. R. (2025). DFT analysis on electronic properties, reactivity and adsorption mechanism of favipiravir/XTiO_2 (X = Pt, Zr, Zn) nanocomplexes and their biological evaluations. *Trends in Sciences*, 22(9):10384.

Mamand, D. (2019). Theoretical calculations and spectroscopic analysis of Gaussian computational examination-NMR, FTIR, UV-Visible, MEP on 2, 4, 6-nitrophenol. *Journal of Physical Chemistry and Functional Materials*, 2(2):77–86.

Mulliken, R. S. (1955). Electronic population analysis on LCAO-MO molecular wave functions.

Murray, S. and Sen, K. (1996). *Molecular Electrostatic Potentials: Concepts and Applications.*

Murugavel, K., Amirthaganesan, S., Rajamohan, R., Bharanidharan, S., and Mohan, T. S. (2023). Synthesis and spectral studies of some polysubstituted cyclohexanone oximes; DFT approach for the optimization. *Journal of Molecular Structure*, 1283:135299.

O'Boyle, N. M., Tenderholt, A. L., and Langner, K. M. (2008). GaussSum: A graphical user interface for molecular orbital visualization and analysis. *Journal of Computational Chemistry*, 29:839–845.

Padmanabhan, J., Parthasarathi, R., Subramanian, V., and Chattaraj, P. K. (2007). Electrophilicity based charge transfer descriptor. *The Journal of Physical Chemistry A*, 111:1358–1361.

Pandey, B. K., Pandey, S. K., and Pandey, D. (2011). A survey of bioinformatics applications on parallel architectures. *International Journal of Computer Applications*, 23(4):21–25.

Pearson, R. G. (1989). Absolute electronegativity and hardness: applications to organic chemistry. *Journal of Organic Chemistry*, 54:1423–1430.

Ramalingam, S., Karabacak, M., Periandy, S., Puviarasan, N., and Tanuja, D. (2012). Spectroscopic (infrared, Raman, UV and NMR) analysis, Gaussian hybrid computational investigation (MEP maps/HOMO and LUMO) on cyclohexanone oxime. *Spectrochimica Acta Part A: Molecular and Biomolecular Spectroscopy*, 96:207–220.

Rijal, R., Lamichhane, H. P., and Pudasainee, K. (2022). Molecular structure, HOMO-LUMO analysis and vibrational spectroscopy of the cancer healing pro-drug temozolomide based on DFT calculations. *AIMS Biophysics*, 9(3):208–220.

Saji, R. S., Prasana, J. C., Muthu, S., and George, J. (2021). Experimental and theoretical spectroscopic (FT-IR, FT-Raman, UV-Vis) analysis, natural bonding orbitals and molecular docking studies on 2-bromo-6-methoxynaphthalene: A potential anti-cancer drug. *Heliyon*, 7(6):e07213.

Sánchez-Márquez, J., Zorrilla, D., Sánchez-Coronilla, A., de los Santos, D., Navas, J., Fernández-Lorenzo, C., Alcántara, R., and Martín-Calleja, J. (2014). Introducing "UCA-Fukui" software: reactivity-index calculations. *Journal of Molecular Modeling*, 20:2492.

Sharp, J., Ciotti, A., Andrews, H., Udayasurian, S. R., García-Melchor, M., and Li, T. (2024). Sustainable electrosynthesis of cyclohexanone oxime through nitrate reduction on a ZnCu alloy catalyst. *ACS Catalysis*, 14(5):3287–3297.

Spectrochimica Acta Part A: Molecular and Biomolecular Spectroscopy, 114:220–230.

St, M. and Flett, C. (1957). Infrared spectra of organic compounds: The oxime group. *Spectrochimica Acta Part A*, 10:21–25.

Sumathi, T., Anandhan, B., Nithya, R., and Kamatchi, S. (2025). Synthesis and spectral studies of novel cyclohexanone-based derivatives and their biological activity. *Journal of Molecular Structure*, 1338:142285.

Sumathi, T., Nithya, R., Kamatchi, S., and Ramanathan, P. (2024). Synthesis, spectral analysis, DFT and molecular docking studies of some novel oxime derivatives. *Chemical Physics Impact*, 8:100583.

The Journal of Chemical Physics, 23(10):1833–1840.

Unger, P. D. and McMahon, F. J. (1981). High-performance liquid chromatography of cyclohexanone oxime in urine and plasma. *Journal of Chromatography*, 210:360–364.

W. (2010). Revealing noncovalent interactions. *Journal of the American Chemical Society*, 132(18):6498–6506.

Yoshida, H., Ehara, A., and Matsuura, H. (2000). Density functional vibrational analysis using wavenumber-linear scale factors. *Chemical Physics Letters*, 325(4):477–483.

Zhang, J. S., Riaud, A., Wang, K., Lu, Y. C., and Luo, G. S. (2014). Beckmann rearrangement of cyclohexanone oxime to α-caprolactam in a modified catalytic system of trifluoroacetic acid. *Catalysis Letters*, 144:151–157.